

AD-A178 731

PLASMA JOINING OF METAL MATRIX COMPOSITES(U) MSNM INC  
SAN MARCOS CA G H REYNOLDS ET AL. DEC 86  
ARO-22817. 4-M5-5 DAAG29-85-C-0027

1/1

UNCLASSIFIED

F/G 11/4

NL





UNCLASSIFIED

SECURITY CLASSIFICATION OF THIS PAGE (When Data Entered)

2

REPORT DOCUMENTATION PAGE		READ INSTRUCTIONS BEFORE COMPLETING FORM
1. REPORT NUMBER <b>ARO 22817.4-M5-5</b>	2. GOVT ACCESSION NO. <b>AD-A178731</b> N/A	3. RECIPIENT'S CATALOG NUMBER N/A
4. TITLE (and Subtitle)  <b>PLASMA JOINING OF METAL MATRIX COMPOSITES</b>		5. TYPE OF REPORT & PERIOD COVERED <b>Interim Technical June/July 1986</b>
		6. PERFORMING ORG. REPORT NUMBER N.A.
7. AUTHOR(s)  <b>G.H. Reynolds and L. Yang</b>		8. CONTRACT OR GRANT NUMBER(s)  <b>DAAG29-85-C-0027</b>
9. PERFORMING ORGANIZATION NAME AND ADDRESS  <b>MSNW, Inc. P.O. Box 865 San Marcos, CA 92069</b>		10. PROGRAM ELEMENT, PROJECT, TASK AREA & WORK UNIT NUMBERS
11. CONTROLLING OFFICE NAME AND ADDRESS  <b>U. S. Army Research Office Post Office Box 12211 Research Triangle Park, NC 27709</b>		12. REPORT DATE <b>December 1986</b>
14. MONITORING AGENCY NAME & ADDRESS (if different from Controlling Office)		13. NUMBER OF PAGES <b>11</b>
		15. SECURITY CLASS. (of this report)  <b>Unclassified</b>
16. DISTRIBUTION STATEMENT (of this Report)  <b>Approved for public release; distribution unlimited.</b>		15a. DECLASSIFICATION/DOWNGRADING SCHEDULE
17. DISTRIBUTION STATEMENT (of the abstract entered in Block 20, if different from Report)  <b>NA</b>		
18. SUPPLEMENTARY NOTES  <b>The view, opinions, and/or findings contained in this report are those of the author(s) and should not be construed as an official Department of the Army position, policy, or decision, unless so designated by other documentation.</b>		
19. KEY WORDS (Continue on reverse side if necessary and identify by block number)  <b>Composite materials, joining, plasma processing, thermochemistry.</b>		
20. ABSTRACT (Continue on reverse side if necessary and identify by block number)  <b>The microstructural and microchemical changes produced in precomposited 1100 aluminum - 30 wt.% SiC, aluminum - 5 wt.% Ti - 30 wt.% SiC and aluminum - 3 wt.% Zr - 30 wt.% SiC<sup>p</sup> powder filler metals caused by low pressure, transferred arc plasma deposition<sup>p</sup> onto inert substrates are described.</b>		

DD FORM 1473

EDITION OF 1 NOV 68 IS OBSOLETE

UNCLASSIFIED

SECURITY CLASSIFICATION OF THIS PAGE (When Data Entered)



## ABSTRACT

The microstructural and microchemical changes produced in precomposited 1100 aluminum - 30 wt.%  $\text{SiC}_p$ , aluminum - 5 wt.% Ti - 30 wt.%  $\text{SiC}_p$  and aluminum - 3 wt.% Zr - 30 wt.%  $\text{SiC}_p$  powder filler metals caused by low pressure, transferred arc plasma deposition onto inert substrates are described.

DTIC
COPY
INSPECTED
6
OR
<input checked="" type="checkbox"/>
<input type="checkbox"/>
ON
on/
Availability Codes
11 and/or
Special

## EXPERIMENTAL RESULTS

This report describes microstructural and microchemical characterization of low pressure, transferred arc plasma deposits produced on inert substrates using precomposited powder feed (i. e. filler) materials. Powder preparation and low pressure, transferred arc plasma processing parameters were described in a previous report. Also described in the most recent report were the microchemical differences observed between as-produced precomposited powders and those which had been plasma processed and allowed to solidify in free flight. The plasma deposited composite powders described herein impinged on an inert, stainless steel substrate backed by a water-cooled copper chill block to prevent substrate softening and melting. Three types of precomposited powders were used as feed material. These were 1100 aluminum - 30 wt.%  $\text{SiC}_p$ , aluminum - 5 wt.% Ti - 30 wt.%  $\text{SiC}_p$  and aluminum - 3 wt.% Zr - 30 wt.%  $\text{SiC}_p$ . *Silicon Carbide Powders*

Figure 1 shows the C and Si microprobe traces across a representative  $\text{SiC}$  particle in the microstructure of the 1100 aluminum - 30 wt.%  $\text{SiC}_p$  deposit. The  $\text{SiC}$  particle showed edge X-ray resolution of 4 microns which was slightly lower than reported previously for the as-produced powder. Corrected X-ray intensity ratios for Si and C are 31:1 which is virtually identical to the

starting powder. The average SiC particle size is similar to that of the starting powder unlike that observed in the composite powder allowed to solidify in free flight where substantial fragmentation of the SiC phase within the composite powder particles was observed. It is concluded that microchemical differences between the starting powders and the dense, solid deposits are minimal for this baseline system.

Figure 2 shows C, Si and Ti microprobe traces near and across a representative SiC particle in the microstructure of the dense aluminum - 5 wt.% Ti - 30 wt.% SiC<sub>p</sub> deposit. The Si:C X-ray intensity ratio was 25 in reasonable agreement with the starting powders. The average SiC phase particle size was reduced with respect to the starting powders as previously observed for composite powders allowed to solidify in free flight. Figure 3 shows a second microprobe trace through the same SiC particle. The Si:C ratio was 29.6 in good agreement with the starting powders. For both microprobe traces, Ti-rich phase particles were observed in the matrix alloys unlike the case of the powders allowed to solidify in free flight where the excess titanium was apparently "quenched-in" to the matrix alloy. The slower cooling rate of the solid deposit likely results in Al<sub>3</sub>Ti precipitation and growth in the matrix alloy. The most striking feature of the microprobe traces shown in Figures 2 and 3 is the appearance of an apparent Ti-rich reaction zone at the particle/matrix interface as might be expected under relatively slow cooling conditions. The interfacial phase, probably TiC, is both expected and desired to suppress Al<sub>4</sub>C<sub>3</sub> formation at the interface. A backscattered electron image of the SiC particle and the paths of the two microprobe traces shown in Figures 2 and 3 is shown in Figure 4. The white second phase visible in the matrix is the Ti-rich phase.

Figure 5 and 6 show the C, Si and Zr microprobe traces across a representative SiC particle in the microstructure of the aluminum - 3 wt.% Zr - 30 wt.% SiC<sub>p</sub> deposit and the corresponding backscattered electron image of the SiC particle and trace path, respectively. Similarly, Figures 7 and 8 show C, Si and Zr microprobe traces across a different SiC particle in the same microstructure and the trace path, respectively. (Figures 5 and 6 are at a magnification of 4000X, Figures 7 and 8 at 2000X). The average size of the SiC phase particles was reduced compared to the starting powders as noted above for the Ti-containing matrix alloy. The Si:C X-ray intensity ratios were 33 and 32 for these two particles, which values are similar to the starting materials. A Zr-rich phase, likely Al<sub>3</sub>Zr, is observed in the matrix microstructure as in the starting powders. No Zr-rich region was detected at the particle/matrix interface unlike the case for the Ti-containing matrix composition. The thickness of this region is predicted to be substantially below the resolution limit of the microprobe for the short plasma residence times employed in this study, however, and even after relatively slow cooling in the deposits may still be below the resolution limit.

Thus low pressure, transferred arc plasma processing had no detrimental effect on either the baseline or reactive metal-containing matrix alloy composite compositions. (The reduction in SiC particle size in the plasma deposited material is not considered detrimental). The possible formation of protective, reactive metal rich interfacial phases may be quite beneficial to the properties of the composite deposits. Similar analyses of composite deposits produced on aluminum-SiC<sub>p</sub> composite substrate base plates will be initiated shortly.

# CAMECA-MICROBEAM

08-SEP-85

## STEP SCANNING

AUTO SCALE

Polar Angle = 0

SP1 : ODP8

Max = 1483

Lambda = 44.89 Angstrom

SP2 : PET

Max = 45606

Lambda = 7.13 Angstrom

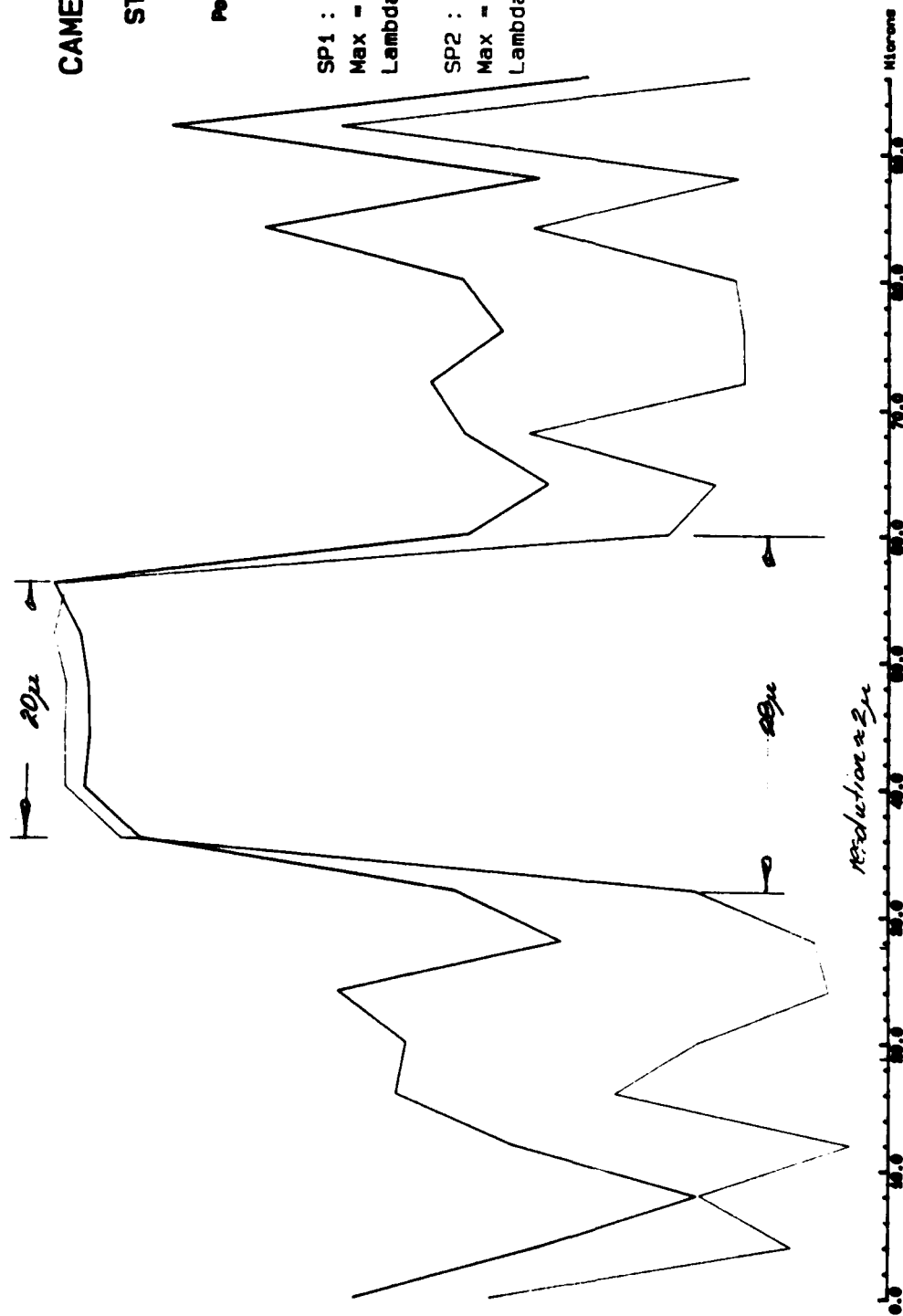


Figure 1.

#2 Sprayed on plate; 1100 + 30% SiC; 15Kv; 10 nAmp; No Photo

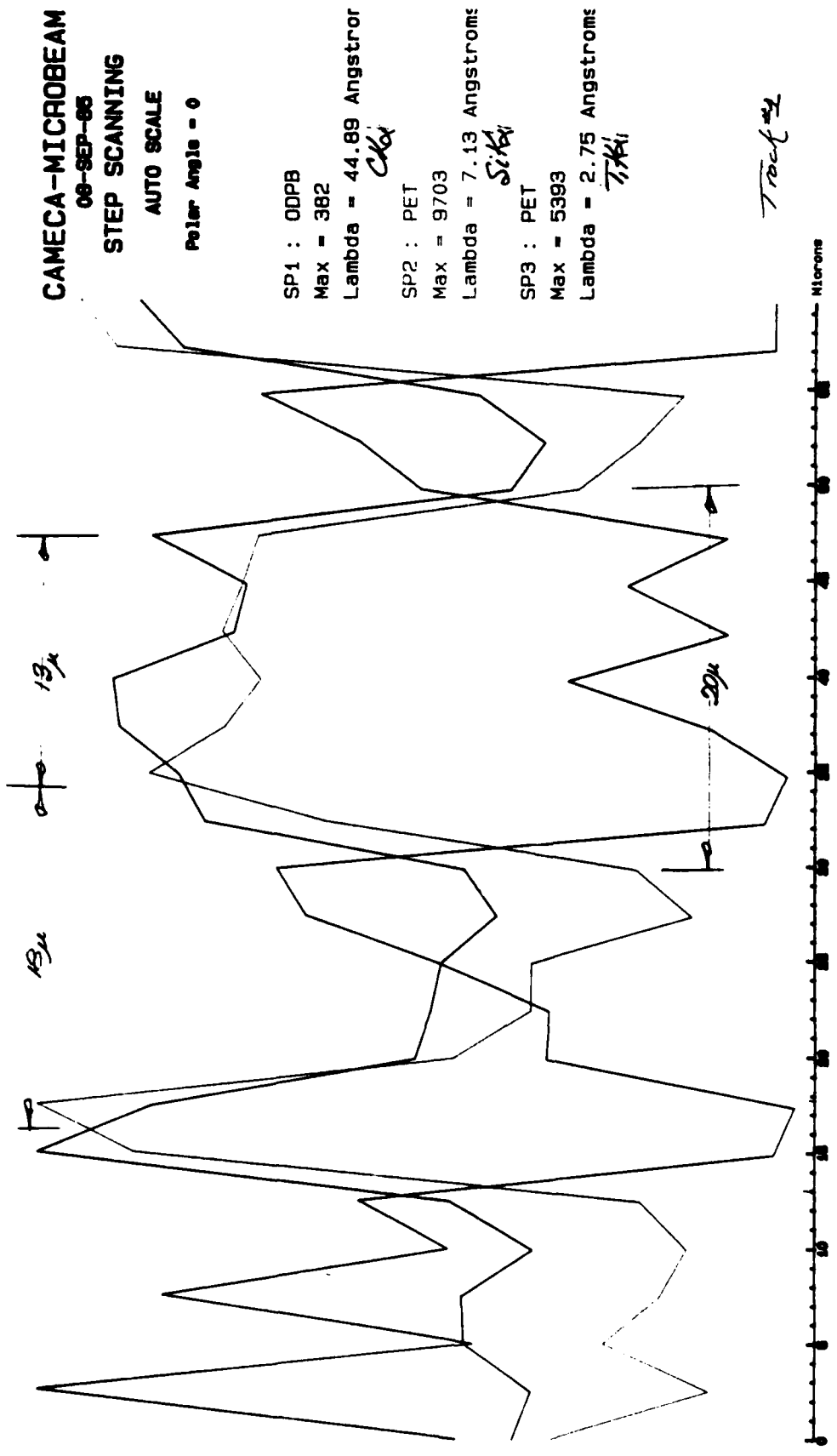


Figure 2.

#2. Sprayed on plate; Al 57 + 30% Si; Cl<sub>K</sub>; Si<sub>K</sub>; Ti<sub>K</sub>; 15kV; 2.1 mm; Backscattered electron; mag = 2000x #2



**CAMECA-MICROBEAM**

08-SEP-80

## STEP SCANNING

**AUTO SCALE**

**Polar Angle = 0**

**SP1 : ODPB**

Max - 943

**Lambda = 44.89 Angstrom**

24

SP2 : PET

Max = 27487

$$\lambda = 7.13 \text{ Angstroms}$$

5.12

SP3 : PET

Max = 14217

**Lambda = 2.75 Angstroms**

1972  
1973

Track #2

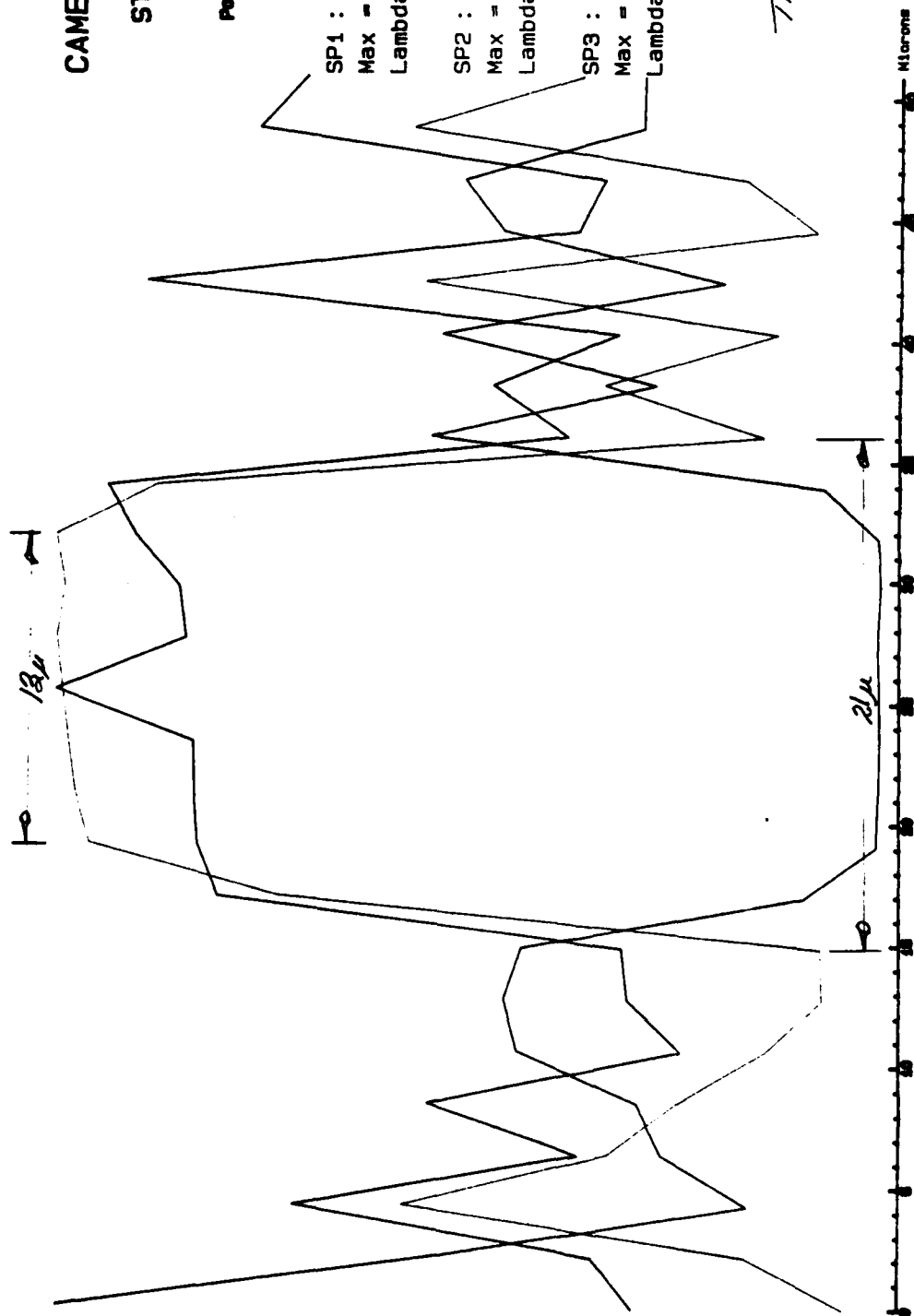


**Figure 3.**

#2-Sprayed on Al<sub>2</sub>O<sub>3</sub>; Al<sub>2</sub>SiTi + 30% SiC; SiK<sub>2</sub>; TiK<sub>2</sub>; 15KV; 5.9 nAmp; Backscattered ~1/2-thru; 100µg = 2000K

42



Figure 4. Backscattered electron image showing the paths of the microprobe traces shown in Figures 2 and 3.

Lo Box of

# CAMECA-MICROBEAM

08-SEP-85

## STEP SCANNING

AUTO SCALE

Polar Angle = 0

SP1 : ODPB

Max = 1500

Lambda = 44.89 Angstrom

SP2 : PET

Max = 49334

Lambda = 7.13 Angstroms

SP3 : PET

Max = 903  $\approx 3.7\%$

Lambda = 8.07 Angstroms

ZrK $\alpha$

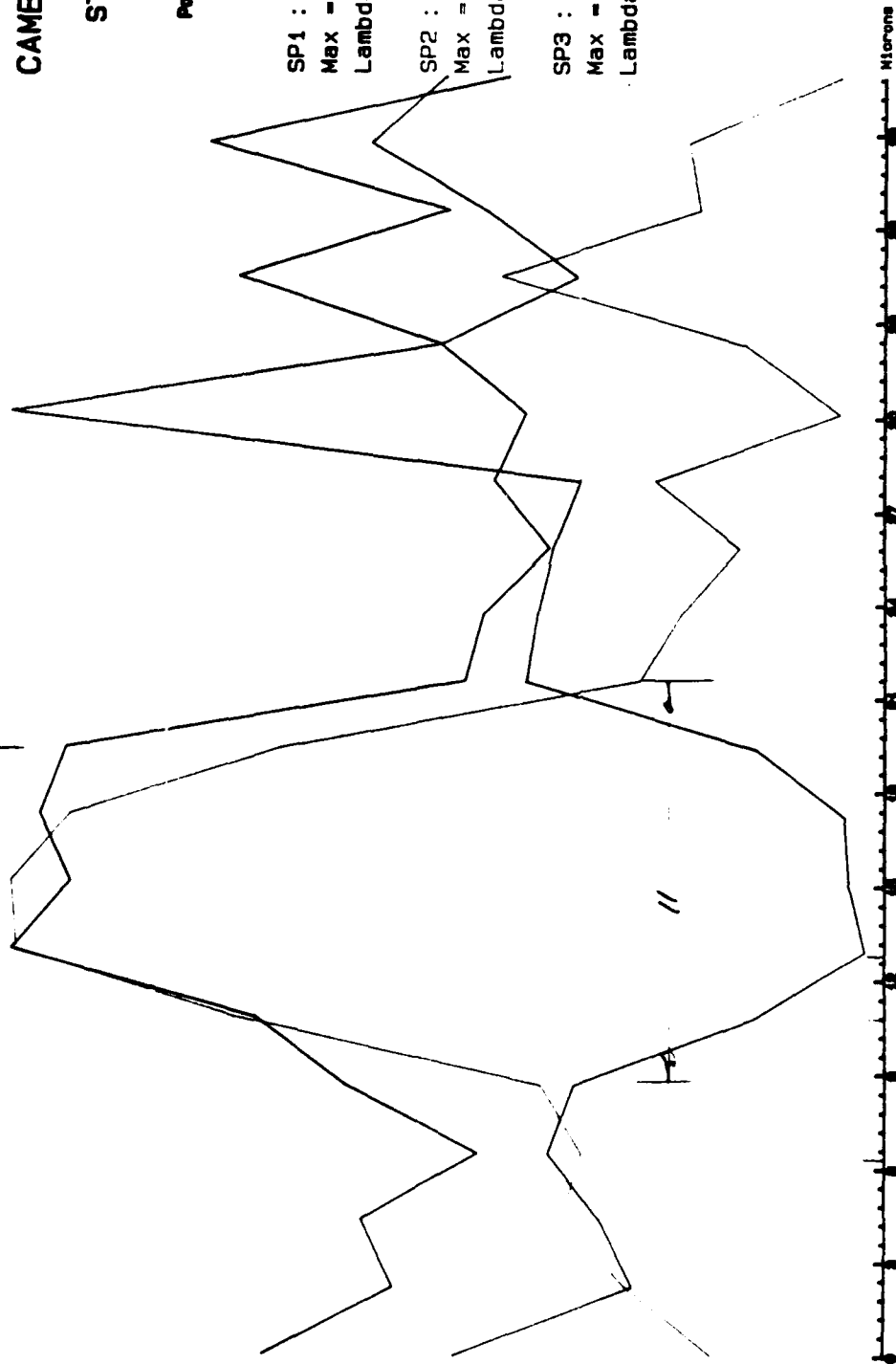


Figure 5.

Track #1

#2 Scanned on Plate: Al 3Zr+30% SiC; SiK $\alpha$ ; SiK $\beta$ ; ZrK $\alpha$ ; 15K $\alpha$ ; 10XMMIP; Backscattered electron; 1100X

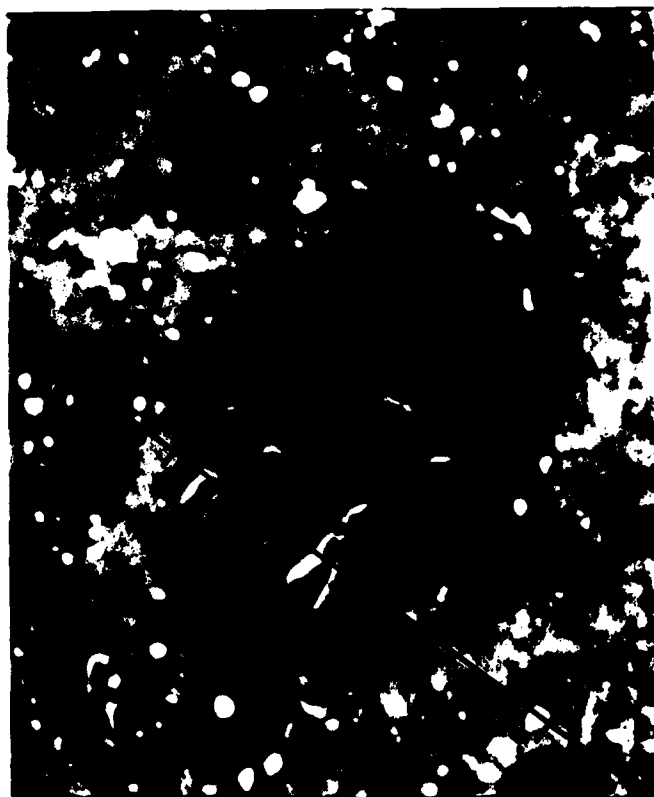


Figure 6. Backscattered electron image showing the path of the microprobe traces shown in Figures 5.

**CAMECA-MICROBEAM**

09-SEP-86

## STEP SCANNING

**AUTO SCALE**

0 - 01 MAY 1964

SP1 : 00P8

Max - 1557

**Lambda = 44.89 Angstrom**

SP2 : PET

Max - 49433

$\lambda = 7.13 \text{ Angstroms}$

SP3 : PET

Max = 3316

**Lambda = 6.07 Angstroms**

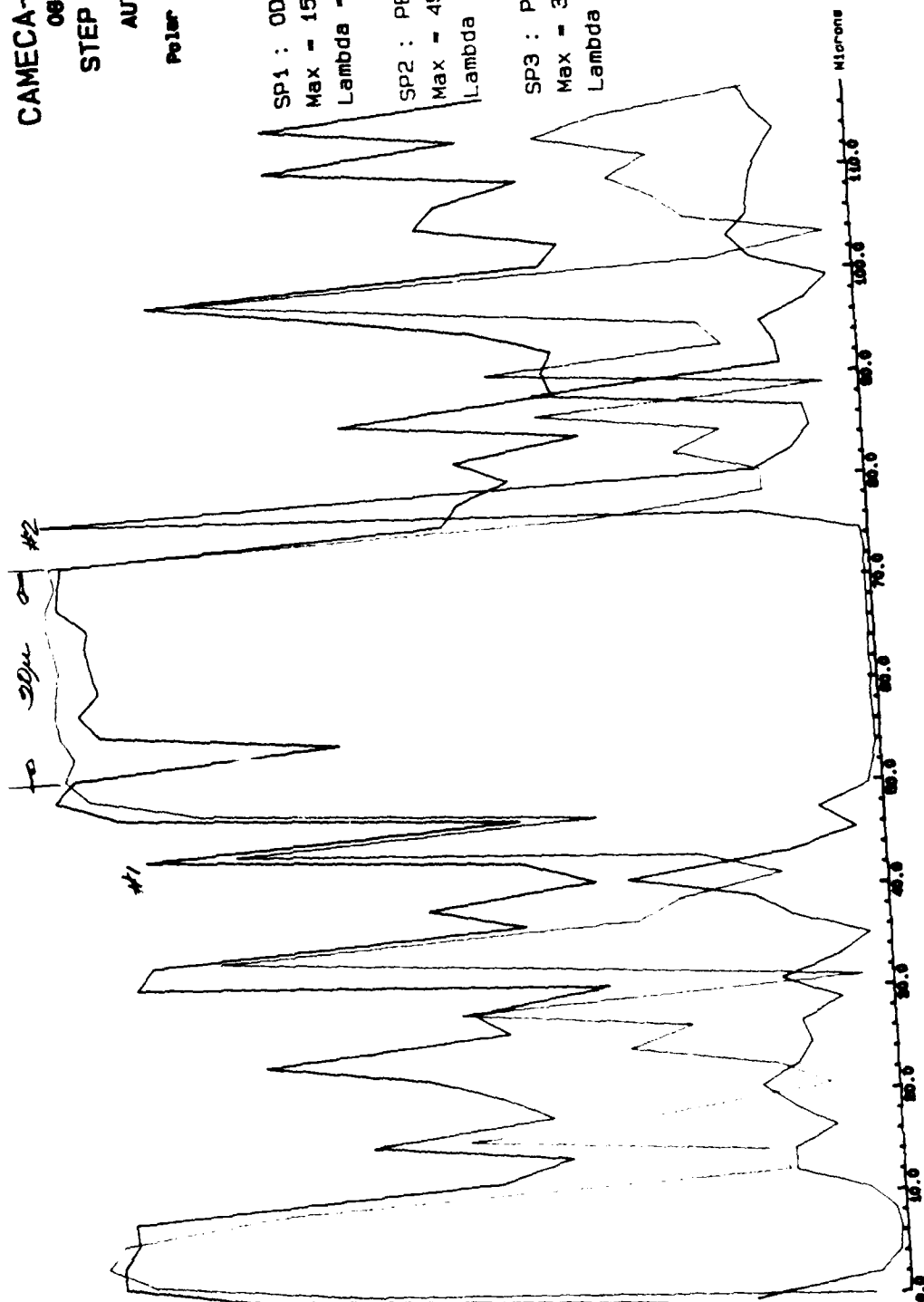


Figure 7.

Trail #2

24

$\therefore 1149 = 2200K$



Figure 8. Backscattered electron image showing the path of the microprobe traces shown in Figures 7.

END

5-87

DTIC